

On the effect of “glancing” collisions in the cold atom vacuum standard

Stephen P. Eckel ^{1, a)} Daniel S. Barker ¹ James A. Fedchak ¹ Jacek Kłos ^{2, 3} Julia Scherschligt ¹ and Eite Tiesinga ^{2, 3, 4}

¹⁾*Sensor Science Division, National Institute of Standards and Technology, Gaithersburg, Maryland 20899, USA*

²⁾*Joint Quantum Institute, College Park, Maryland 20742, USA*

³⁾*Physics Department, University of Maryland, College Park, Maryland, 20742, USA*

⁴⁾*Quantum Measurement Division, National Institute of Standards and Technology, Gaithersburg, Maryland 20899, USA*

(Dated: 18 September 2024)

We theoretically investigate the effect of “glancing” collisions on the ultra-high vacuum (UHV) pressure readings of the cold atom vacuum standard (CAVS), based on either ultracold ^7Li or ^{87}Rb atoms. Here, glancing collisions are those collisions between ultracold atoms and room-temperature background atoms or molecules in the vacuum that do not impart enough kinetic energy to eject an ultracold atom from its trap. Our model is wholly probabilistic and shows that the number of the ultracold atoms remaining in the trap as a function of time is non-exponential. We update the recent results of a comparison between a traditional pressure standard—a combined flowmeter and dynamic expansion system—to the CAVS [D.S. Barker, *et al.*, *AVS Quantum Science* **5** 035001 (2023)] to reflect the results of our model. We find that the effect of glancing collisions shifts the theoretical predictions of the total loss rate coefficients for ^7Li colliding with noble gases or N_2 by up to 0.6 %. Likewise, we find that in the limit of zero trap depth the experimentally extracted loss rate coefficients for ^{87}Rb colliding with noble gases or N_2 shift by as much as 2.2 %.

I. INTRODUCTION

Cold atom vacuum standards measure vacuum pressures by observing the loss rate of cold, “sensor” atoms from a shallow, conservative trap due to collisions with background gases at temperature T and number density n .^{1–15} Most collisions impart sufficient energy ΔE such that the total energy E of the sensor atom after the collision is larger than the trap depth W , causing a sensor atom to be ejected from the trap and lost. If all collisions result in loss, then the sensor atom loss is exponential in time with loss rate $\Gamma = Kn$, where K is the collision rate coefficient with SI unit cm^3/s and n with SI unit cm^{-3} . However, some collisions are “glancing”: they do not impart enough energy to eject an atom from the trap. These glancing collisions represent an important systematic effect for CAVS-based vacuum pressure measurements.

How to treat systematics due to the glancing collisions has been a matter of discussion in the literature. The simplest means to assess systematics is to assume, as done implicitly in Refs. 9–11, 14–19, (1) that the temperature of the sensor atom cloud T_S is zero, and (2) that glancing collisions do not change the energy of a sensor atom. Under these two assumptions, sensor atom loss is still exponential but now with rate $\Gamma = Kn[1 - P_A(W)]$, where $P_A(\Delta E)$ is the cumulative probability that a collision adds a positive energy less than ΔE to the sensor atom’s kinetic energy in the trap. (See App. A for an explanation of the kinematics and the sign of ΔE .) Various theoretical expressions for $P_A(W)$ exist in the literature. For example, Ref. 14 gives $P_A(W) = (a_{\text{gl}}W + b_{\text{gl}}W^2)/K$ by appropriately factoring Eq. 1 in their paper. Other expressions can be found in Refs. 9–13, 20–22.

Estimates show that if ^{87}Rb is used as a sensor atom, $P_A(W)$ is of the order of 10 % for most collision partners at $T = 300\text{ K}$ and $W/k_B \sim 1\text{ mK}$, where k_B is the Boltzmann constant.

For ^7Li sensor atoms, $P_A(W)$ is about an order of magnitude smaller. Reference 12 addressed the first of these two assumptions and derived a modified form for the observed loss rate for $T_S > 0$. Reference 20 relaxed the second of these two assumptions in the context of Rb+Rb collisions, numerically calculating a glancing-collision corrected measurement of the C_6 van-der-Waals coefficient assuming the universality of quantum diffractive collisions (UQDC). Likewise, Ref. 23 relaxed both assumptions and found that the measured collision rates could be shifted by as much as 3 % for Ar background atoms colliding with ^{87}Rb .

A recent comparison by the current authors between cold atom vacuum standards and a classical vacuum metrology apparatus showed uncertainties approaching 1 %, ¹⁵ but used the two simplistic assumptions described above to fit for K and the first two terms of the Taylor expansion of $P_A(\Delta E)$ in terms of ΔE . At the 1 % level of accuracy, the effect of two glancing collisions per sensor atom within a time $t \lesssim 3/\Gamma$ is important for ^{87}Rb , because $[P_A(W)]^2 \sim 1\%$. This glancing collision effect was not included in the uncertainty budget of Ref. 15.

Inspired by the developments of Refs. 12, 20, and 23, we strive to create a comprehensive and fully analytic model of glancing collisions in the CAVS. We structure our model, described in Sec. II, in terms of two probabilities: the probability for a sensor atom to have a collision with a background gas atom or molecule and the probability of that collision to cause the sensor atom to acquire kinetic energy $E > W$; causing that atom to be ejected from the trap. We show that under certain conditions, the loss of sensor atoms from the trap becomes non-exponential. In Sec. IV, we correct the recent data of Ref. 15 based on our analytic model. In App. A, we give a brief review of the kinematics, while in App. B, we refine the estimate of the temperature of the ^{87}Rb cloud used in Ref. 15.

^{a)}Electronic mail: stephen.eckel@nist.gov

II. PROBABILISTIC MODEL OF SENSOR-ATOM LOSS

Our probabilistic model of atom loss begins by noting that the ultracold sensor atom clouds are dilute and far away from quantum degeneracy, i.e., the average time between collisions among sensor atoms is much longer than $1/(Kn)$ and thus the sensor-atom cloud is effectively a non-interacting gas of atoms. For the ^7Li gases in Ref. 15, the rate of collisions between sensor atoms $\beta \approx K_S n_S \sim 10^{-6} \text{ s}^{-1}$ at the maximum possible number densities of $n_S \sim 10^6 \text{ cm}^{-3}$ and rate coefficient $K_S \approx 1.5 \times 10^{-12} \text{ cm}^3/\text{s}$. This rate is much smaller than any measured Γ in the UHV domain by Ref. 15. For the ^{87}Rb gases in Ref. 15, $\beta \approx 0.03 \text{ s}^{-1}$, when averaged over the entire, non-uniform density of the cloud using a peak density of $n_S \approx 1.6 \times 10^{-9} \text{ cm}^{-3}$, a temperature $T_S = 53(11) \text{ } \mu\text{K}$ (see App. B), and $K_S \sim 1.2 \times 10^{-10} \text{ cm}^3/\text{s}$. This rate is a factor of two smaller than the smallest measured Γ in Ref. 15. We thus need only to construct a probabilistic loss model for an ensemble of traps, each containing a single sensor atom. An atom has one or more collisions with atoms or molecules in the vacuum before it leaves its trap.

The experimental design of traps for ultracold atoms has a significant impact on the equilibrium or initial $t = 0$ probability distribution of the atoms. First, as mentioned before, these traps have a finite depth W but, in addition, in the process of cooling the sensor atoms the experimentalists use what is informally called a ‘‘knife’’ that removes any atom with a motional energy larger than cut-off energy E_c that is often significantly lower than W . Moreover, the trapping potential $U(\mathbf{r})$ as function of location \mathbf{r} limits the spatial excursions of the atoms. Assuming that the potential energy of the trap is smallest at $\mathbf{r} = \mathbf{0}$ and that $U(\mathbf{0}) = 0$, the cumulative probability of a sensor atom having an energy less than E is given by

$$P_0(E) = \int_0^E dE' \rho(E') e^{-E'/k_B T_S}, \quad (1)$$

where $\rho(E)$ is the density of states and depends on the shape of $U(\mathbf{r})$. For a separable, power law potential of the form

$$U(x, y, z) = c_1 |x|^p + c_2 |y|^q + c_3 |z|^s, \quad (2)$$

where $p, q, s > 0$, $|x|$ is the absolute value of real x , and $c_i > 0$ for $i = 1, 2$, and 3 , the density of states obeys^{24–26}

$$\rho(E) \propto E^{1/2+1/p+1/q+1/s} \equiv E^{1/2+\delta}. \quad (3)$$

Equation (1) can then be evaluated analytically and is

$$P_0(T_S, E_c, E) = \frac{\gamma(3/2 + \delta, E/k_B T_S)}{\gamma(3/2 + \delta, E_c/k_B T_S)} \quad (4)$$

when $E < E_c$ and 1 otherwise. Here, $\gamma(a, x) = \int_0^x y^{a-1} e^{-y} dy$ is the incomplete gamma function.

For a magneto-optical trap (MOT) with its linear trapping force and thus quadratic potential along all three spatial dimensions, $\delta = 3/2$. For a magnetic quadrupole trap with constant trapping force and thus a linear potential along all three spatial axes, $\delta = 3$. For a constant or box potential, $\delta = 0$.

The sensor-atom clouds created in Ref. 15 were last in thermal equilibrium in a MOT, and thus we anticipate that $\delta = 3/2$. Subsequent measurements, described in App. B, confirm this.

For time $t > 0$, we observe that the cumulative probability $P_R(E, t)$ for an atom in the ensemble to have total energy less than E can be expressed in terms of the expansion

$$P_R(E, t) = p_0^{(c)}(t) P_0(T_S, E_c, E) + p_1^{(c)}(t) P_1(T_S, E_c, E) + p_2^{(c)}(t) P_2(T_S, E_c, E) + \dots, \quad (5)$$

where $p_k^{(c)}(t)$ is the probability that a sensor atom has experienced $k = 0, 1, 2, \dots$ collisions with background gas atoms or molecules after time t . Collisions between a sensor atom and background atoms and molecules occur at random times with a timescale of $1/(Kn)$. The distribution of collision times is then Poissonian and

$$p_k^{(c)}(t) = \frac{1}{\Gamma(k+1)} (Knt)^k e^{-Knt}, \quad (6)$$

where $\Gamma(z)$ is the Gamma function.

Cumulative probability $P_0(E, T_S, E_c)$ is defined in Eq. (4) and, more generally, $P_k(E, T_S, E_c)$ are the cumulative probabilities that an atom has total energy less than E after $k = 0, 1, 2, \dots$ collisions. We can derive $P_k(E, T_S, E_c)$ recursively. After the k -th collision, $P_k(E, T_S, E_c)$ is given by the convolution of the probability density $p_A(\Delta E)$ that the collision adds energy $\Delta E > 0$ to the sensor atom and the cumulative probability $P_{k-1}(E', T_S, E_c)$ such that $E = E' + \Delta E$. Following App. A we realize that nearly all collisions add energy to the sensor atoms and assume $p_A(\Delta E) = 0$ for $\Delta E < 0$. Consequently,

$$P_k(T_S, E_c, E) = \int_0^\infty dE' p_A(E - E') P_{k-1}(T_S, E_c, E'). \quad (7)$$

The probability density $p_A(\Delta E)$ is found by noting that

$$\int_0^{\Delta E} d\varepsilon p_A(\varepsilon) \equiv P_A(\Delta E) \quad (8)$$

with cumulative probability $P_A(\Delta E)$ as defined in the introduction. It is reasonable to assume that $p_A(\Delta E)$ and $P_A(\Delta E)$ are independent of the initial collision energy as long as $\Delta E \gg k_B T_S$, with sensor atoms essentially at rest, and index k limited to only a few collisions. As discussed in Refs. 15–17, the change in $P_A(\Delta E)$ due to a finite initial velocity of the ultracold atoms is of the order of $(m/\mu)(T_S/T) \sim 10^{-5}$, where μ is the reduced mass of the collision partners, and is negligible at our level of accuracy.

From the introduction, we also have

$$P_A(\Delta E) = \alpha_1 \Delta E + \alpha_2 \times (\Delta E)^2 + \dots \quad (9)$$

for $\Delta E \geq 0$ with $\alpha_1 = a_{\text{bg}}/K$ and $\alpha_2 = b_{\text{bg}}/K$. Consequently,

$$p_A(\Delta E) = \sum_{i=1}^{\infty} i(\Delta E)^{i-1} \alpha_i \quad (10)$$

for $\Delta E \geq 0$ and zero otherwise. We have used K , a_{gl} , and b_{gl} from Ref. 14, reproduced in Table III for ^{87}Rb , and realize

System	α_1/k_B (mK ⁻¹)	α_2/k_B^2 (mK ⁻²)
⁸⁷ Rb-H ₂	0.037	-0.002
⁸⁷ Rb-He	0.014	-0.00028
⁸⁷ Rb-Ne	0.053	-0.003
⁸⁷ Rb-N ₂	0.076	0.0068
⁸⁷ Rb-Ar	0.079	-0.0072
⁸⁷ Rb-Kr	0.11	-0.014
⁸⁷ Rb-Xe	0.14	-0.024

TABLE I. Values of coefficients α_i for ⁸⁷Rb sensor atoms with $i = 1$ and 2 in Eq. (9) derived from the theory of Ref. 14. No uncertainties are presented as the table is only meant to indicate relative sizes of the α_i . Values for α_i with $i > 2$ are currently unknown and assumed to be zero in our simulations.

that the $P_A(\Delta E)$ are much smaller than one for the relevant ΔE . Table I lists values for ⁸⁷Rb sensor atoms. Typical trap depths are of order $k_B \times 1$ mK and we realize that $\alpha_2 W^2 \ll \alpha_1 W \ll 1$. For ⁷Li sensor atoms these inequalities also hold. An alternative choice from Refs. 10–12, 20, and 22 results in $\alpha_j = \beta_j / (U_d)^j$, where $U_d = 4\pi\hbar^2 / [m(K/\langle v \rangle)]$ is the median energy exchanged in the collision with mean velocity $\langle v \rangle = \sqrt{k_B T / 2M}$ for a background gas species with mass M . Here, \hbar is the reduced Planck constant. Coefficients β_j are given in Table 1 of Ref. 10.

The probabilities $P_i(T_S, E_c, E)$ can be evaluated using the chapter on the confluent hypergeometric function found in Ref. 27 after we express the incomplete gamma function in terms of the Kummer's confluent hypergeometric function. After some thought, we obtain

$$P_1(T_S, E_c, E) = \sum_{i=1}^{\infty} \alpha_i (k_B T_S)^i \left\{ \begin{array}{ll} \mathcal{M}_i \left(\frac{3}{2} + \delta, \frac{E_c}{k_B T_S}, \frac{E}{k_B T_S} \right) & E < E_c \\ \sum_{k=0}^i \binom{i}{k} \left(\frac{E - E_c}{k_B T_S} \right)^k \mathcal{M}_{i-k} \left(\frac{3}{2} + \delta, \frac{E_c}{k_B T_S}, \frac{E_c}{k_B T_S} \right) & E \geq E_c \end{array} \right. , \quad (11)$$

where $\binom{i}{k}$ is the binomial coefficient, dimensionless function

$$\begin{aligned} \mathcal{M}_i(a, x_c, x) &\equiv i \int_0^x d\varepsilon (x - \varepsilon)^{i-1} \frac{\gamma(a, \varepsilon)}{\gamma(a, x_c)} \quad (12) \\ &= x^i \left(\frac{x}{x_c} \right)^a \frac{\Gamma(i+1) \mathbf{M}(a, a+i+1, -x)}{\mathbf{M}(a, a+1, -x_c)} \quad (13) \end{aligned}$$

and Kummer's (regularized) confluent hypergeometric function $\mathbf{M}(a, b, z)$ is defined in Eqs. (13.2.E3) and (13.2.E4) of Ref. 27. In the derivation of Eq. (13), we have also used Eqs. (13.6.E5) and (13.4.E2) of this reference. We observe that Eq. (13) allows us to define $\mathcal{M}_i(a, x_c, x)$ for $i = 0$ and realize that $\mathcal{M}_0(a, x_c, x_c) = 1$. Finally, note that

$$\mathcal{M}_i(a, x_c, x_c) \rightarrow x_c^i \left(1 - i \frac{a}{x_c} + O(1/x_c^2) \right) \quad (14)$$

for $x_c \rightarrow +\infty$ based on Eq. (13.7.E2) of Ref. 27. Consequently,

focusing on $E \approx W$ and realizing that $k_B T_S \ll E_c < W$, we have

$$P_1(T_S, E_c, E) \rightarrow \sum_{i=1}^{\infty} \alpha_i \left[\sum_{k=0}^i \binom{i}{k} (E - E_c)^k E_c^{i-k} \right. \quad (15)$$

$$\left. - (3/2 + \delta) k_B T_S \sum_{k=0}^i \binom{i}{k} (i-k) (E - E_c)^k E_c^{i-k-1} \right] \\ = \sum_{i=1}^{\infty} \alpha_i E^i \left[1 - (3/2 + \delta) i \frac{k_B T_S}{E} \right] \quad (16)$$

$$= P_A(E) - (3/2 + \delta) k_B T_S P_A(E), \quad (17)$$

where in the formula in square brackets we recognize the binomial formula and its derivative.

Next, we derive

$$P_2(T_S, E_c, E) = \sum_{j=1}^{\infty} \sum_{i=1}^{\infty} \alpha_j \alpha_i (k_B T_S)^{i+j} \frac{\Gamma(i+1)\Gamma(j+1)}{\Gamma(i+j+1)} \left\{ \begin{array}{ll} \mathcal{M}_{i+j} \left(\frac{3}{2} + \delta, \frac{E_c}{k_B T_S}, \frac{E}{k_B T_S} \right) & E < E_c \\ \sum_{k=0}^{i+j} \binom{i+j}{k} \left(\frac{E - E_c}{k_B T_S} \right)^k \mathcal{M}_{i+j-k} \left(\frac{3}{2} + \delta, \frac{E_c}{k_B T_S}, \frac{E_c}{k_B T_S} \right) & E \geq E_c \end{array} \right. \quad (18)$$

again using Eq. (13.4.E2) of Ref. 27. Again focusing on $E \approx W$ and realizing that $k_B T_S \ll E_c < W$, we have

$$P_2(T_S, E_c, E) \rightarrow \sum_{j=1}^{\infty} \sum_{i=1}^{\infty} \alpha_j \alpha_i \frac{\Gamma(i+1)\Gamma(j+1)}{\Gamma(i+j+1)} E^{i+j} = \frac{1}{2} \alpha_1^2 E^2 + \frac{2}{3} \alpha_1 \alpha_2 E^3 + \dots \quad (19)$$

as we again recognized a binomial formula in $E - E_c$ and E_c . We also observe that $P_2(T_S, E_c, E) \approx [P_A(E)]^2 / 2$.

For completeness, we have

$$P_3(T_S, E_c, E) = \sum_{l=1}^{\infty} \sum_{j=1}^{\infty} \sum_{i=1}^{\infty} \alpha_l \alpha_j \alpha_i (k_B T_S)^{i+j+l} \quad (20)$$

$$\times \frac{\Gamma(i+1)\Gamma(j+1)\Gamma(l+1)}{\Gamma(i+j+l+1)} \left\{ \begin{array}{ll} \mathcal{M}_{i+j+l} \left(\frac{3}{2} + \delta, \frac{E_c}{k_B T_S}, \frac{E}{k_B T_S} \right) & E < E_c \\ \sum_{k=0}^{i+j+l} \binom{i+j+l}{k} \left(\frac{E-E_c}{k_B T_S} \right)^k \mathcal{M}_{i+j+l-k} \left(\frac{3}{2} + \delta, \frac{E_c}{k_B T_S}, \frac{E_c}{k_B T_S} \right) & E \geq E_c \end{array} \right.$$

The expressions for $P_k(T_S, E_c, E)$ for $k = 4, 5, \dots$ follow by inspection from Eqs. (11), (18), and (20). For $k_B T_S \ll E_c < E$ we then derive

$$P_k(T_S, E_c, E) \approx \frac{1}{\Gamma(k+1)} \alpha_1^k E^k \left(1 - k(3/2 + \delta) \frac{k_B T_S}{E} \right) \quad (21)$$

$$+ \frac{2k}{\Gamma(k+2)} \alpha_1^{k-1} \alpha_2 E^{k+1} \left(1 - (k+1)(3/2 + \delta) \frac{k_B T_S}{E} \right)$$

for $k = 0, 1, \dots$ leading to an approximate analytical expression for the time evolution of the cumulative probability for an atom in the ensemble to have total energy less than E that is given by

$$P_R^{\text{approx}}(E, t) = e^{-Knt} \left\{ I_0(2y) - (3/2 + \delta) \frac{k_B T_S}{E} y I_1(2y) \right. \\ \left. + 2 \frac{\alpha_2 E}{\alpha_1} \left(1 - 2(3/2 + \delta) \frac{k_B T_S}{E} \right) I_2(2y) \right. \\ \left. - 2(3/2 + \delta) \frac{\alpha_2 k_B T_S}{\alpha_1} y I_3(2y) \right\} \quad (22)$$

with $y = \sqrt{\alpha_1 E K n t}$ and is thus non-exponential in time. Here, $I_n(z)$ is the modified Bessel function of the first kind, $I_n(z) \rightarrow (z/2)^n / \Gamma(n+1)$ for $z \rightarrow 0$, and $I_n(z) \rightarrow e^z / \sqrt{2\pi z}$ for $z \rightarrow \infty$. Equations (21) and (22) form two of the main analytical results of this article.

Two further, less accurate approximations for the cumulative probability $P_R(E, t)$ are relevant to compare with previous work. We can find these approximations by rewriting Eqs. (5) and (6) in the equivalent cumulant form

$$P_R(E, t) = P_0 e^{-(1-P_1/P_0)Knt + (P_0 P_2 - P_1^2)(Knt)^2 / (2P_0^2) + O(t^3)} \quad (23)$$

suppressing the three arguments of the cumulative probabilities $P_k(T_S, E_c, E)$ for clarity. The terms proportional to t^2 , t^3 , etc in the exponential lead to non-exponential behavior. If only assumption (2) holds, *i.e.* glancing collisions do not change the energy of an atom, then the cumulative probability that an atom survives i uncorrelated collisions is equal to the probability that an atom survives one collision raised to the i th power. This corresponds to the choice $P_k(T_S, E_c, E) = [P_1(T_S, E_c, E)]^k$ for $k = 0, 1, 2, \dots$ and only the term linear in t in Eq. (23) survives leading to

$$P_R^{(1)}(E, t) = e^{-[1-P_1(T_S, E_c, E)]Knt}, \quad (24)$$

equivalent to the result of Ref. 12. When both assumptions hold, we have $P_k(T_S, E_c, E) = [P_A(E)]^k$ for $k = 0, 1, 2, \dots$ and

$$P_R^{(A)}(E, t) = e^{-[1-P_A(E)]Knt} \quad (25)$$

used in Refs. 11, 13–15, respectively. With Eq. (22), we have shown that the exponential time evolutions in Eqs. (24) and (25) are only valid up to first order in $P_A(E)$ or, more precisely, up to first order in $\alpha_1 E$.

Finally, we note that the fraction of remaining trapped sensor atoms in the ensemble $\eta_S(t)$ is given by $\eta_S(t) = P_R(E = W, t)$.²⁸ Inspection, remembering that $E_c \leq W$, shows that $\eta_S(t = 0) = 1$. For future use, we define a measure of non-exponential behavior by

$$\Xi(W, t) = |P_2(T_S, E_c, W) - [P_1(T_S, E_c, W)]^2| Knt \quad (26)$$

based on the ratio of the t^2 and t terms in Eq. (23), where we have used that $P_0(T_S, E_c, W) = 1$ and $P_1(T_S, E_c, W) \ll 1$ for our sensor atoms.

III. VISUALIZATION OF THE PROBABILISTIC MODEL

Figure 1(a) shows the exact and approximate cumulative probabilities $P_k(T_S, E_c, E)$ scaled by $(\alpha_1 E)^k$ for $k = 1, 2$ and 3 as functions of E for ^{87}Rb sensor atoms and a Xe background gas using α_1 and α_2 derived from data in Ref. 14, reproduced in our Table III, with parameters $\delta = 3/2$, $E_c/k_B = 0.2$ mK and $T_S = 53$ μK that are motivated by the experiments of Ref. 15 and discussed in App. B. For the largest E shown in the figure, $P_A(E) \approx \alpha_1 E \approx 0.2$. We find that, for $E \gg E_c$ and all three k , the approximate expression in Eq. (21) approaches the exact expression as expected. Moreover, $P_k(T_S, E_c, E) / [P_A(T_S, E_c, E)]^k < 1$ for all k and E shown, representing a breakdown of the approximation $P_k(T_S, E_c, E) = [P_A(E)]^k$ and, consequently, assumptions (1) and (2) described in the introduction.

Figure 1(b) shows $P_R(E, t)$, computed from Eq. (5) and our exact expressions for $P_k(T_S, E_c, E)$, as functions of E for various hold times t . As in Ref. 20, the curves have a non-continuous derivative at $E = E_c$. For $E < E_c$, $P_R(t, E)$ is mostly determined by the initial cumulative distribution $P_0(T_S, E_c, E)$ of atoms in the trap and the probability with time that these atoms have not undergone a collision $p_0^{(c)}(t)$. For $E > E_c$, $P_R(t, E)$ is independent of E at $t = 0$, indicating no

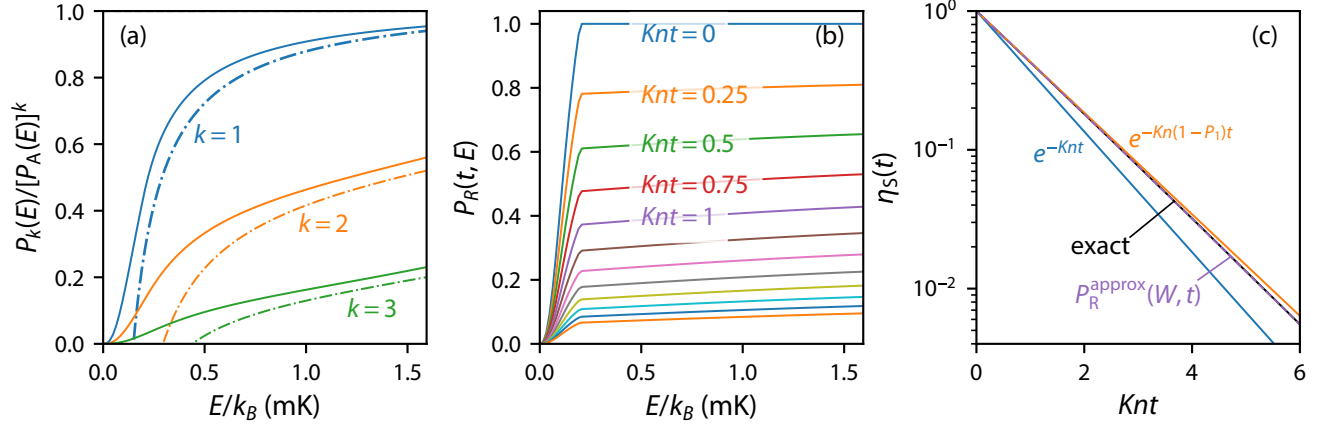


FIG. 1. (a) Exact and approximate scaled cumulative probabilities $P_k(T_S, E_c, E)/[P_A(E)]^k$ for ^{87}Rb sensor atoms having an energy less than E after $k = 1, 2, 3$ collisions with Xe background gas atoms in blue, orange, and green, respectively. We use the $P_A(\Delta E)$ from Ref. 14 and assume $\delta = 3/2$, $T_S = 53 \mu\text{K}$, and $E_c/k_B = 0.2 \text{ mK}$. Solid curves are based on the exact expressions in Eqs. (11), (18), and (20). Dot-dashed curves are based on Eq. (21) extrapolated to $E = 0$. (b) Exact cumulative probabilities $P_R(E, t)$ of ^{87}Rb sensor atoms as functions of E at several hold times t based on Eq. (5) using the exact expressions for $P_k(T_S, E_c, E)$. From top to bottom colors encode $Knt = 0$ to 2.5 in steps of 0.25. System parameters are the same as those in panel (a). (c) Fractional remaining sensor-atom number $\eta_S(t) = P_R(W, t)$ as functions of Knt with trap depth $W = 1.5940 \text{ mK}$ and other system parameters as in panel (a). The solid black curve corresponds to Eq. (5) with the exact expressions for $P_k(T_S, E_c, E)$. The approximation in Eq. (22) is shown as the dashed purple curve. The solid orange curve shows the approximate prediction of Eq. (24). Finally, the solid blue curve shows $\eta_S(t) = e^{-Knt}$ for the “ideal” CAVS, where $W \rightarrow 0$.

population at these total energies, while for $t > 0$, it acquires an increasing positive slope $dP_R(t, E)/dE$ with t , indicating the build up of hotter atoms that have experienced one or more glancing collisions.

The exact remaining fraction of atoms $\eta_S(W, t) = P_R(W, t)$ as well as several approximations are shown in Fig. 1(c) with $W = 1.5940(2) \text{ mK}$ and other system parameters as in panels (a) and (b). The exact curve for $\eta_S(W, t)$ lies significantly above the exponential loss curve e^{-Knt} of the “ideal” CAVS in the limit $W \rightarrow 0$ and lies only slightly below the exponential loss curve of Eq. (24). The non-exponential prediction of Eq. (22) is nearly indistinguishable from the exact result (5), with about a 1.5 % error at $Knt = 6$.

To further validate our analytical calculations, we perform Monte-Carlo simulations of sensor atom loss. The simulations begin at $t = 0$ with 10^6 sensor atoms at initial energies chosen at random according to $P_0(T_S, E_c, E)$ in Eq. (4). After every time step $\Delta t = 0.005 \times (1/Kn)$, chosen such that $Kn\Delta t \ll 1$, a random number in the interval $[0, 1)$ is chosen for each atom and if that number is smaller than $Kn\Delta t$, then the sensor atom undergoes a collision with a background gas molecule. For sensor atoms undergoing collisions, a random energy ΔE according to the probability density in Eq. (10) is chosen and is added to the sensor atom’s current energy. If a sensor atom’s new energy is larger than W , the sensor atom is ejected, *i.e.* removed from the ensemble of sensor atoms in the Monte-Carlo simulations. Cumulative probability distributions $P_k^{(\text{MC})}(T_S, E_c, E)$, $P_R^{(\text{MC})}(E, t)$, and $\eta_S^{(\text{MC})}(W, t)$ for the Monte-Carlo simulations are then constructed. The Monte Carlo simulations and our exact results agree; *i.e.*, the curves for the system parameters used in Fig. 1 can not be distinguished on the scales of the three panels in the figure.

IV. EFFECT ON THE RECENT COMPARISON BETWEEN CLASSICAL AND QUANTUM STANDARDS

Decay curves $\eta_S(t)$ in the experiments of Ref. 15 were measured for both ^7Li and ^{87}Rb sensor atoms colliding with near-room-temperature $X = \text{He, Ne, N}_2, \text{Ar, Kr, and Xe}$ background gases introduced into the CAVSs at a known number density n . The time evolution of the decay curves was then fit to an exponential with loss rate Γ , which was assumed to be of the form $\Gamma = Ln = Kn[1 - P_A(W)]$ with $P_A(W) = (a_{\text{gl}}W - b_{\text{gl}}W^2)/K$. This form for Γ is only valid under assumptions (1) and (2), described in the introduction.

Let us first consider the effect of violating these assumptions on the ^7Li -X collision data, which were taken at trap depth $W = k_B \times 0.95(14) \text{ mK}$, leading to $\alpha_1 W \ll 1$ as the α_1 for ^7Li are two orders of magnitude smaller than those for ^{87}Rb sensor atoms. The measured exponential decay rates Γ as functions of n were fit assuming $\Gamma = Ln$ to extract an observed rate coefficient L . The fitted L was then compared to the predicted value obtained with quantum mechanical scattering calculations of Ref. 14. Both theory and experiment relied on assumptions (1) and (2). We thus need to correct the theoretical predictions of L given the finite T_S and characterize potential systematic shifts due to non-exponential decay on the extracted L for ^7Li .

To update the theoretical predictions of L , we need an accurate estimate of the temperature T_S for ^7Li . A convenient value of $T_S = 0.1 \text{ mK}$ was used in Ref. 15, which was not necessarily reflective of the actual temperature. In fact, T_S is not well known. Here, we take a much larger ^7Li temperature of $T_S = 0.75 \text{ mK}$ from a temperature measurement of such atoms in a MOT in a similar apparatus.²⁹ We conservatively assume a standard uncertainty of 0.25 mK and observe that $k_B T_S \approx W$.

System	L (thr)	L (exp)	$E_n(L)$
	($10^{-9}\text{cm}^3/\text{s}$)	($10^{-9}\text{cm}^3/\text{s}$)	
$^7\text{Li}-^4\text{He}$	1.66(4)	1.72(3)	0.63
$^7\text{Li}-\text{Ne}$	1.55(14)	1.634(16)	0.28
$^7\text{Li}-\text{N}_2$	2.65(2)	2.67(3)	0.33
$^7\text{Li}-\text{Ar}$	2.34(1)	2.38(2)	0.95
$^7\text{Li}-\text{Kr}$	2.150(7)	2.20(3)	0.65
$^7\text{Li}-\text{Xe}$	2.25(2)	2.22(3)	-0.45

TABLE II. Theoretical (thr) and updated experimentally (exp) determined loss rate coefficients L for various natural abundance gases colliding with ultracold ^7Li sensor atoms. The theoretical values are based on the exponential time evolution in Eq. (24) with $T_S = 0.75(25)$ mK, $E_c = W = k_B \times 0.95(14)$ mK, and K , a_{gl} and b_{gl} from Ref. 14. The last column shows the degree of equivalence $E_n(L) = (L_{\text{exp}} - L_{\text{thr}})/[2u(L_{\text{exp}} - L_{\text{thr}})]$. All uncertainties are one-standard deviation $k = 1$ uncertainties.

We also take $E_c = W$, and, since the last time the cloud was in thermal equilibrium was in the MOT, we have $\delta = 3/2$.

Next, we realize that for the special case $E_c = W = k_B T_S$ and $\delta = 3/2$ the cumulative probabilities $P_k(T_S, E_c, W)$ are

$$\begin{aligned} P_1(W/k_B, W, W) &= \frac{11 - 4e}{2e - 5} \alpha_1 W + O(W^2) \quad (27) \\ &= 0.290 \dots \alpha_1 W + O(W^2) \end{aligned}$$

and

$$\begin{aligned} P_2(W/k_B, W, W) &= \frac{7e - 19}{2e - 5} (\alpha_1 W)^2 + O(W^3) \quad (28) \\ &= 0.0640 \dots (\alpha_1 W)^2 + O(W^3). \end{aligned}$$

Equation (27) implies that with $k_B T_S \approx E_c = W$, as in our ^7Li experiments, $P_1(T_S, W, W)$ is about three times smaller than $P_A(W)$. This can be compared to $P_1(T_S, E_c, W) = P_A(W)$ when $k_B T_S \ll E_c < W$ analyzed in the previous section. Thus, glancing collisions are less of a concern than assumed in Ref. 15. Physically, because $k_B T_S \approx W$, it is easier for ^7Li atoms to be ejected from the trap.

Secondly, our measure for non-exponential behavior $\Xi(W, t) = |P_2 - P_1^2|(Knt) \approx 0.02(\alpha_1 W)^2 Knt$ is at most 10^{-5} for all background gases at the largest $Knt = 4$ measured in Ref. 15. Consequently, at our level of accuracy for extracting loss rates Γ for ^7Li , contributions from non-exponential decay can be neglected and the rate coefficient $L = K[1 - P_1(T_S, E_c, W)]$ with $P_1(T_S, E_c, W)$ from Eq. (27) can be used. Because $0 < P_1(T_S, E_c, W) < P_A(W)$, the theoretically predicted values for L are larger than those in Ref. 15. Moreover, the contribution to the uncertainty of L from W is reduced compared to that in Ref. 15. The updated predictions for L , shown in Table II, are now in better agreement with their experimental counterparts, with the theoretical and experimental values agreeing at two standard deviations ($k = 2$).

An updated uncertainty budget for $^7\text{Li}-\text{Ar}$ and the change in the theoretical predictions of L from Ref. 15 are shown in the Supplemental Tables S1 and S2, respectively. The maximum change in L from Ref. 15 is 0.64 % for $^7\text{Li}+\text{Xe}$. In fact, for all background gases the change in L is less than our updated corresponding theoretical uncertainty.

The situation is more complicated for ^{87}Rb sensor atoms. Once again, we require a better estimate of the sensor-atom temperature T_S . It is now obtained by measuring the energy distribution of the ^{87}Rb atoms in the quadrupole trap as in Ref. 20 and described in App. B. We find $T_S = 53(12)$ μK ensuring that we are in the limit $k_B T \ll E_c < W$ studied in Sec. II.

In Ref. 15, exponential decay was assumed for the loss of ^{87}Rb sensor-atoms. For $k_B T \ll E_c < W$, the measure of non-exponential behavior $\Xi(W, t) \approx 0.50(\alpha_1 W)^2 Knt$ is largest for a Xe background gas at $\Xi(W, t) = 0.028$ using the longest experimental hold time. This value is comparable to the fractional standard statistical uncertainty $u(\Gamma)/\Gamma$ for the decay rates Γ found from exponential fits to $\eta_S(t)$ versus t . Thus, we refit the data of Ref. 15 to account for non-exponential decay.

For our fit, let us first consider the exact solution in Eq. (5) with the substitutions of $\eta_S(t) = \eta_0 P_R(W, t)$ and $\Gamma_0 = Kn$, which yields

$$\eta_S(t) = \eta_0 e^{-\Gamma_0 t} \left[1 + P_1(\Gamma_0 t) + \frac{1}{2} P_2(\Gamma_0 t)^2 + \frac{1}{6} P_3(\Gamma_0 t)^3 + \dots \right]. \quad (29)$$

with probabilities $P_k(\cdot, \cdot, \cdot)$ evaluated at $E = W$. One immediate question arises: how many $P_k(T_S, E_c, W)$ must be included given our measurement uncertainties in $\eta_S(t)$? Using a second convenient substitution of $\Gamma_i = Kn\alpha_i = \Gamma_0\alpha_i$ for $i = 1, 2, \dots$ together with our approximate expression for $P_k(T_S, E_c, W)$ in Eq. (21), we find

$$\begin{aligned} \eta_S(t) &\approx e^{-\Gamma_0 t} \left\{ 1 + \sum_{i=1}^2 \Gamma_i W^i \left(1 - i(3/2 + \delta) \frac{kT_S}{W} \right) t \right. \quad (30) \\ &\quad \left. + \left[\frac{1}{4} (\Gamma_1 W)^2 + \frac{1}{3} \Gamma_1 \Gamma_2 W^2 \right] t^2 + \frac{1}{36} (\Gamma_1 W)^3 t^3 + \dots \right\}. \end{aligned}$$

Thus, we observe that the dominant coefficient for each t^k in the braces $\{\dots\}$ is $(\Gamma_1 W)^k / [\Gamma(k+1)]^2$. For the data of Ref. 15, the maximum W for which data was taken is $W/k_B = 1.6$ mK and the maximum t was approximately $3/\Gamma_0$. At $t = 3/\Gamma_0$, the measured relative uncertainty $u(\eta_S(t))/\eta_S(t) \gtrsim \varepsilon \equiv 0.05$. We then demand that $(3\Gamma_1 W/\Gamma_0)^k / [\Gamma(k+1)]^2 < 0.01\varepsilon$ to ensure convergence of the series in Eq. (29). Using the theoretical prediction for $^{87}\text{Rb}-\text{Xe}$ of Ref. 14, which has the largest Γ_1 of all studied background gases, this requirement demands computing terms up to and including $k = 4$.

The data of Ref. 15 is further complicated by apparent two-body losses. We thus fit the normalized ^{87}Rb atom number $\eta_S(W, t)$ as a function of t and W for given T_S , E_c , and background gas number density n to the numerical solution of

$$\frac{d\eta_S}{dt} = -\Gamma(W, t)\eta_S - \beta(W)\eta_S^2, \quad (31)$$

with $\eta_S(t=0) = \eta_0$, where the trap depth and time dependent $\Gamma(W, t)$ is

$$\Gamma(W, t) = -\frac{d \log P_R(W, t)}{dt} = -\frac{1 + \sum_{i=1}^4 P_i t^{i-1} / \Gamma(i)}{1 + \sum_{i=1}^4 P_i t^i / \Gamma(i+1)} \quad (32)$$

and the two-body loss parameter $\beta(W) = \beta_0 + \beta_1 W$. We have verified that the numerical solution of Eq. (31) using the second equality of Eq. (32) reproduces Eq. (29) to better than 0.0001ε , where $\varepsilon = 0.05$ as before.

For each value of n , the authors of Ref. 15 measured time traces $\eta_S(W, t)$ between $t = 0$ and $t \approx 4/\Gamma_0$ for seven W between $k_B \times 0.4$ mK and $k_B \times 1.6$ mK. The sensor atom temperature and cutoff energy are fixed at $T_S = 53(12)$ μ K and $E_c = k_B \times 0.1993(2)$ mK, respectively. Moreover, we assume $\delta = 3/2$. The quality of the experimental data determines the number of Γ_i included in the fit. We use Γ_i for $i = 1, \dots, i_{\max}$, where i_{\max} is the first value of i that satisfies $\Gamma_{i_{\max}} < 2u(\Gamma_{i_{\max}})$ and $u(\Gamma_i)$ is the statistical standard uncertainty in Γ_i . Consequently, for $^{87}\text{Rb-He}$ the adjusted parameters are η_0 , Γ_0 , Γ_1 , β_0 , and β_1 . For all others systems, Γ_2 is the sixth adjusted parameter. We propagated the 20 % uncertainty of T_S through the fits by determining $d\Gamma_i/dT_S$ for $i = 0, \dots, i_{\max}$. The $< 0.1\%$ uncertainties of E_c and W are negligible contributions to our total uncertainty. The fitted $\beta(W) > 0$ at a $2\text{-}\sigma$ ($k = 2$) uncertainty for 33 % of our time traces, possibly indicating the presence of two body collisional induced loss. For the remaining fits, $\beta(W)$ is consistent with zero at $2\text{-}\sigma$.

By construction for each background gas, fitted quantities Γ_i with $i = 0, \dots, i_{\max}$ should only be proportional to the background gas number density n . We, however, observe offsets as function of n and thus obtain rate coefficients K and glancing collision rates a_{gl} and b_{gl} for the roughly 10 values of n between $4 \times 10^7 \text{ cm}^{-3}$ and $4 \times 10^9 \text{ cm}^{-3}$ using

$$\begin{aligned}\Gamma_0 &= Kn + \Gamma_{0,\text{base}}, \\ \Gamma_1 &= a_{\text{gl}}n + \Gamma_{1,\text{base}}, \\ \Gamma_2 &= b_{\text{gl}}n + \Gamma_{2,\text{base}}.\end{aligned}\quad (33)$$

with offsets $\Gamma_{i,\text{base}}$ as two additional adjusted parameters for $^{87}\text{Rb-He}$ and three additional adjusted parameters for all others background gases. In these second, linear fits, we have accounted for the uncertainties of and covariances among the two or three Γ_i obtained by fitting the time traces as well as the roughly 0.3 % relative uncertainty in n . Rate $\Gamma_{0,\text{base}}$ is $0.027(6) \text{ s}^{-1}$ independent of the background gas species $\Gamma_{1,\text{base}}$ and $\Gamma_{2,\text{base}}$ are consistent with zero at $2\text{-}\sigma$ in 70 % of the fits and at $3\text{-}\sigma$ for all of the fits. It is likely that $\Gamma_{0,\text{base}}$ is caused by residual gas, likely H_2 , at our base or lowest pressure. Assuming H_2 gas with $K_{\text{H}_2} = 3.9(1) \times 10^{-9} \text{ cm}^3/\text{s}$ ¹⁴, we derive $n_{\text{base}} = \Gamma_{0,\text{base}}/K_{\text{H}_2} = 6.9(1.5) \times 10^6 \text{ cm}^3/\text{s}$, corresponding to base pressure $p_{\text{base}} = n_{\text{base}}k_B T = 2.8(6) \times 10^{-8} \text{ Pa}$, in agreement with those extracted from decay curves measured at $n = 0$ in Ref. 15. If the $\Gamma_{i,\text{base}}$ for $i = 1$ and 2 are also caused by H_2 gas and if $\Xi(W, t) \ll 1$ for all t for both the residual gas and the species of interest, then we can show that $\Gamma_{1,\text{base}} = a_{\text{gl},\text{base}}n_{\text{base}}$ and $\Gamma_{2,\text{base}} = b_{\text{gl},\text{base}}n_{\text{base}}$. The corresponding fit values of a_{gl} and b_{gl} are consistent with the expected values of $a_{\text{gl}} \approx 1.4 \times 10^{-7} \text{ cm}^3/(\text{s K})$ and $b_{\text{gl}} \approx 8 \times 10^{-5} \text{ cm}^3/(\text{s K}^2)$ for H_2 , but also consistent with zero within at a $2\text{-}\sigma$ ($k = 2$) uncertainty.

Table III shows the comparison between the updated ^{87}Rb experimental values for K , a_{gl} , and b_{gl} and the corresponding original theoretical values of Ref. 14. Generally the experi-

mental values are now in better agreement with the theory. As with the results of Ref. 15, all numbers agree at two-standard deviations ($k = 2$) except K for $^{87}\text{Rb-Ar}$, which agrees only at four-standard deviations ($k = 4$), and a_{gl} for $^{87}\text{Rb-Kr}$, which agrees at three standard deviations ($k = 3$). Supplemental Tables S3, S4, and S5 show a sample uncertainty budget for $^{87}\text{Rb-Ar}$, the change in the values of K , a_{gl} , and b_{gl} from Ref. 15 to this work, and the current state of knowledge for values of K , respectively. The maximum relative change in K is -2.2% for $^{87}\text{Rb-Xe}$, as expected given that Xe results in the most glancing collisions.

V. CONCLUSION

We have developed a probabilistic and analytic model of glancing collisions in a CAVS. While inspired by the recent semiclassical results of Ref. 12 and 20, our model can use either semiclassical scattering theory^{10–12,20,22} or fully quantum mechanical scattering theory^{14,16–19} as an input. We use our model to update the values of Ref. 15 based on a more complete description of the time evolution of the number of ultracold sensor atoms. We find that our relative adjustments for the theoretically predicted L for $^7\text{Li-X}$ are $\lesssim 0.6\%$. For $^{87}\text{Rb-X}$, we find that our relative adjustments are as large as 2.2 % for our experimental, extrapolated zero-trap depth loss rate coefficients, K . Importantly, we note that a CAVS based on ^7Li is far less sensitive to the initial temperature of the cold atom cloud and the effects of glancing collisions than one based on ^{87}Rb . A CAVS based on ^{87}Rb can compensate for such complications, but requires ancillary measurements to achieve high levels of accuracy.

Appendix A: Collision kinematics and timescales

In this appendix, we briefly review the kinematics of collisions in the context of ultracold sensor atoms of mass m held in a trap with potential energy $U(\mathbf{r})$ at location \mathbf{r} colliding with room-temperature background atoms or molecules. The minimum potential energy occurs at $\mathbf{r} = \mathbf{0}$ and $U(\mathbf{r} = \mathbf{0}) = 0$. Therefore, total energy $E = 0$ is the lowest energy of an atom in the trap, which occurs when it is at rest at $\mathbf{r} = \mathbf{0}$. Atoms with $E > 0$ execute classical orbits starting from position \mathbf{r} and velocity \mathbf{v} such that $E = m|\mathbf{v}|^2/2 + U(\mathbf{r})$ is conserved. For large \mathbf{r} , potential $U(\mathbf{r})$ approaches trap depth W from below along at least one direction \mathbf{r} . Typical timescales for orbits of atoms with magnetic moment μ in a quadrupole magnetic trap are $\tau_{\text{orbit}} \sim \sqrt{2mk_B T_S}/(\mu B')^2$, where atom temperature $T_S \ll W/k_B$, $\mu \approx \mu_B$, μ_B is the Bohr magneton, and B' is the magnetic field gradient of the quadrupole trap. In our CAVSs, τ_{orbit} is of the order of 1 ms. If an atom is executing an orbit with $E > W$, it is not bound by the trap and is ejected.

The sensor atom and background particle do not move appreciably during the collision. This can be seen by noting that the duration of a collision is $\tau_{\text{collision}} \sim \sqrt{\sigma_{\text{eff}}}/\langle v \rangle$, where $\langle v \rangle$ is

System	K (thr)	K (exp)	$E_n(K)$	a_{gl} (thr)	a_{gl} (exp)	$E_n(a_{\text{gl}})$	b_{gl} (thr)	b_{gl} (exp)	$E_n(b_{\text{gl}})$
	($10^{-9}\text{cm}^3/\text{s}$)	($10^{-9}\text{cm}^3/\text{s}$)		($10^{-7}\text{cm}^3/[\text{s K}]$)	($10^{-7}\text{cm}^3/[\text{s K}]$)		($10^{-5}\text{cm}^3/[\text{s K}^2]$)	($10^{-5}\text{cm}^3/[\text{s K}^2]$)	
$^{87}\text{Rb-}^4\text{He}$	2.37(3)	2.35(6)	-0.18	0.336(5)	-0.42(85)	0.44	0.067(3)	—	—
$^{87}\text{Rb-Ne}$	2.0(2)	2.21(5)	0.54	1.06(9)	1.2(7)	-0.09	0.59(3)	2.0(3.5)	-0.21
$^{87}\text{Rb-N}_2$	3.45(6)	3.56(8)	0.54	2.6(2)	1.9(1.4)	0.24	2.3577(7)	5.8(7.2)	-0.24
$^{87}\text{Rb-Ar}$	3.035(7)	3.29(5)	2.38	2.42(2)	2.6(8)	-0.11	2.19(2)	-2.4(3.9)	0.60
$^{87}\text{Rb-Kr}$	2.787(10)	2.80(4)	0.23	3.04(2)	1.8(5)	1.18	3.97(3)	3.8(2.5)	0.02
$^{87}\text{Rb-Xe}$	2.880(10)	2.87(6)	-0.08	4.11(5)	3.5(1.0)	0.30	7.1(1)	12.8(4.5)	-0.64

TABLE III. Theoretical¹⁴ (thr) and updated experimental (exp) values for the loss rate coefficient K at zero trap depth, the first-order glancing rate coefficient a_{gl} , and the second-order glancing rate coefficient b_{gl} for various natural abundance gases colliding with ultracold ^{87}Rb atoms. Numbers in parentheses are one-standard-deviation, $k = 1$ uncertainties. The degree of equivalence is $E_n(K) = (K_{\text{exp}} - K_{\text{thr}})/[2u(K_{\text{exp}} - K_{\text{thr}})]$ for K and likewise for a_{gl} and b_{gl} .

the mean velocity of the background gas atom or molecule at temperature T and $\sigma_{\text{eff}} = K/\langle v \rangle \equiv \pi d_{\text{eff}}^2$ is the effective cross section of the collision. That is, $\tau_{\text{collision}}$ is related to the time it takes to traverse the effective diameter d_{eff} of the collision partners near room temperature. Given that $K \sim 10^{-9} \text{ cm}^3/\text{s}$ and $\langle v \rangle \sim 10^4 \text{ cm/s}$, we find that $\tau_{\text{collision}} \sim 10 \text{ ps} \ll \tau_{\text{orbit}}$.

A consequence of the large difference in timescales $\tau_{\text{collision}}$ and τ_{orbit} is that collisions occur at well-defined locations. Thus, the change in energy for a sensor atom with initial velocity \mathbf{v}_S and final velocity $\mathbf{v}_S + \delta\mathbf{v}_S$ colliding at location \mathbf{r} with a background gas particle is

$$\begin{aligned} \Delta E &= U(\mathbf{r}) + \frac{1}{2}m(\mathbf{v}_S + \delta\mathbf{v}_S)^2 - \left[U(\mathbf{r}) + \frac{1}{2}m\mathbf{v}_S^2 \right] \\ &= \frac{1}{2}m(\delta\mathbf{v}_S)^2 + m\mathbf{v}_S \cdot \delta\mathbf{v}_S. \end{aligned} \quad (\text{A1})$$

For most collisions and even most glancing collisions $|\delta\mathbf{v}_S| \gg |\mathbf{v}_S|$ as $T_S \ll T$ and $k_B T_S \ll W$, respectively. Furthermore, the bombardment from background gas particles is isotropic and thus the second term in Eq. (A1) is zero when averaged over all possible orientations of $\delta\mathbf{v}_S$. We conclude that the ‘‘average’’ collision adds positive energy $\Delta E = m(\delta\mathbf{v}_S)^2/2$ to the sensor atom’s orbit and that most glancing collisions with background gas particles, *i. e.* those with $\Delta E < W$, heat the sensor-atom cloud.

Appendix B: Refined estimate of the temperature of ultracold ^{87}Rb samples

In this appendix, we describe an updated temperature measurement T_S of the ultracold ^{87}Rb cloud. We use a technique similar to that in Ref. 20. Loss rate coefficients between various gases and ^{87}Rb were measured in the laboratory-scale cold-atom vacuum sensor (I-CAVS). As described in Refs. 13 and 15, the I-CAVS contains an ‘‘RF knife,’’ which applies radio-frequency magnetic fields to the atoms to induce spin-flip transitions at specific locations in a magnetic trap defined by the RF frequency ν_{RF} and local Zeeman shift in the trap. In Ref. 15, the RF knife was used to set cutoff energy E_c and trap depth W . To set E_c , a frequency ramp from $\nu_{\text{RF}}^{\text{init}} = 40 \text{ MHz}$ to $\nu_{\text{RF}}^{\text{final}} = 5 \text{ MHz}$ in 1 s removed atoms from the trap with total energy $E > E_c = h\nu_{\text{RF}}^{\text{final}}\{1 - 2mg/(\mu_B B')\} =$

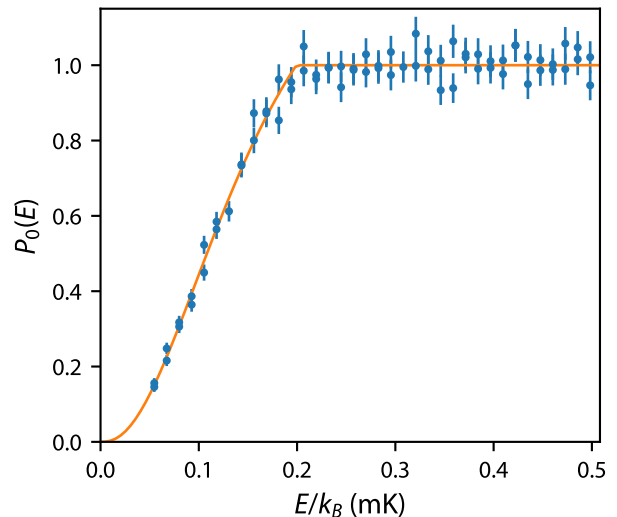


FIG. 2. Experimentally measured $P_0(T_S, E_c, E)$ with standard uncertainties (blue filled circles) for ^{87}Rb sensor atoms as a function of total energy E with cutoff energy $E_c = k_B \times 0.1993(2) \text{ mK}$. The solid orange curve is a fit of the data to Eq. (4) with temperature $T_S = 47(7) \mu\text{K}$ at a fixed value $\delta = 3/2$.

$k_B \times 0.1993(2) \text{ mK}$, where h is Planck’s constant, m is the mass of ^{87}Rb , g is the predicted local gravitational acceleration from Ref. 30, and B' is the measured axial magnetic field gradient of the quadrupole trap. The uncertainty in E_c is limited by our knowledge of B' . Immediately after the ramp, the RF frequency was quickly (essentially instantaneously) changed to a constant, larger value to set trap depth W for the remainder of the measurement.

In this work, we extend our use of the RF knife to measure the initial total-energy distribution $P_0(T_S, E_c, E)$ of ^{87}Rb atoms in the quadrupole magnetic trap as function of total energy E . We follow the procedure described above to prepare the cloud with $E_c = k_B \times 0.1993(2) \text{ mK}$ and subsequently increase the RF frequency to 10 MHz leading to the smallest W used in Ref. 15. In fact, $W = k_B \times 0.3986(4) \text{ mK}$. After holding the atoms in the trap for 10 s at this W , a hold time short compared to typical vacuum lifetimes of roughly 150 s and the typical Rb-Rb collisional thermalization time of roughly 30 s, frequency ν_{RF} is increased to 40 MHz and subsequently

slowly decreased to a value between 100 kHz and 12.5 MHz, ejecting all ^{87}Rb atoms with energy $E > h\nu_{\text{RF}}(1 - 2mg/\mu_B B')$. Finally, we recapture the remaining sensor atoms into a MOT to count them to give $N(E)$ as in Ref. 15. In this way, we measure the distribution $P_0(T_S, E_c, E) = N(E)/N_{\text{init}}$ between $E = k_B \times 3.986(4) \mu\text{K}$ and $k_B \times 0.4982(4) \text{mK} \equiv E_{\text{max}}$, where N_{init} is the sensor atom number just before the frequency of the RF knife is slowly decreased from 40 MHz, which corresponds to $E = E_{\text{init}} \equiv k_B \times 1.5940(2) \text{mK}$. Standard uncertainties in sensor atom number $N(E)$ are taken as in Ref. 15, with the $u(N) = \sqrt{(\sigma_N N^2) + \sigma_0^2}$, with $\sigma_N = 0.04$ and $\sigma_0 = 300$, yielding reduced χ^2_{ν} values near unity and residuals that are independent of E . In practice, as $E_{\text{max}} < E_{\text{init}}$ atom number N_{init} is taken as an adjusted constant.

The results of the measurement of $N(E)$ and thus $P_0(T_S, E_c, E)$ as a function of E for $E_c = k_B \times 0.1993(2) \text{mK}$ are shown in Fig. 2. For $E > E_c$, $P_0(T_S, E_c, E)$ is constant, showing both the effectiveness of the initial sweep of the RF knife to remove “hot” sensor atoms and the lack of a significant number of Rb-Rb rethermalizing collisions during the 10 s hold time. For the present experiment, the RF antenna is less effective at removing ^{87}Rb atoms with $E/k_B \lesssim 0.05 \text{mK}$, so no data are shown in that region. A fit with T_S , δ , and N_{init} as adjusted constants yields $T_S = 59(8) \mu\text{K}$ and $\delta = 1.13(19)$, which includes at 2- σ our expected value of $\delta = 3/2$. A second fit, indistinguishable in Fig. 2, with a fixed and physically motivated value of $\delta = 3/2$, yields $T_S = 47(7) \mu\text{K}$. In an attempt to account for systematic effects, we take as a conservative estimate for T_S the weighted mean of the two estimated temperatures assuming a standard uncertainty given by the temperature difference, which gives $T_S = 53(12) \mu\text{K}$.

ACKNOWLEDGEMENTS

The authors thank K. Madison, J. Booth, and A. Deshmukh for useful discussions; K. Madison and R. Krems for organizing the workshop that helped to elucidate the physics, and P.J. Egan and B. Reschovsky for a thorough reading of the manuscript.

AUTHOR DECLARATIONS

Conflicts of Interest

D.S.B., J.A.F., J.S., and S.P.E. have U.S. patent 11,291,103 issued. D.S.B. and S.P.E. have filed U.S. provisional patent 63/338,047.

DATA AVAILABILITY

The data that support the findings of this study are available from the corresponding author upon reasonable request.

¹J. E. Bjorkholm, “Collision-limited lifetimes of atom traps,” *Phys. Rev. A* **38**, 1599–1600 (1988).

- ²D. E. Fagnan, J. Wang, C. Zhu, P. Djuricanin, B. G. Klappauf, J. L. Booth, and K. W. Madison, “Observation of quantum diffractive collisions using shallow atomic traps,” *Phys. Rev. A* **80**, 022712 (2009).
- ³J. Booth, D. E. Fagnan, B. G. Klappauf, K. W. Madison, and J. Wang, “Method and device for accurately measuring the incident flux of ambient particles in a high or ultra-high vacuum environment,” (2011), US Patent 8,803,072.
- ⁴T. Arpornthip, C. A. Sackett, and K. J. Hughes, “Vacuum-pressure measurement using a magneto-optical trap,” *Phys. Rev. A* **85**, 033420 (2012).
- ⁵J.-P. Yuan, Z.-H. Ji, Y.-T. Zhao, X.-F. Chang, L.-T. Xiao, and S.-T. Jia, “Simple, reliable, and nondestructive method for the measurement of vacuum pressure without specialized equipment,” *Appl. Opt.* **52**, 6195–200 (2013).
- ⁶R. W. G. Moore, L. A. Lee, E. A. Findlay, L. Torralbo-Campo, G. D. Bruce, and D. Cassettari, “Measurement of vacuum pressure with a magneto-optical trap: A pressure-rise method,” *Rev. Sci. Instrum.* **86**, 093108 (2015).
- ⁷V. B. Makhalov, K. A. Martiyanov, and A. V. Turlapov, “Primary vacuum meter based on an ultracold gas in a shallow optical dipole trap,” *Metrologia* **53**, 1287–1294 (2016).
- ⁸J. Scherschligt, J. A. Fedchak, D. S. Barker, S. Eckel, N. Klimov, C. Makrides, and E. Tiesinga, “Development of a new UHV/XHV pressure standard (cold atom vacuum standard),” *Metrologia* **54**, S125 (2017).
- ⁹S. Eckel, D. S. Barker, J. A. Fedchak, N. N. Klimov, E. Norrgard, J. Scherschligt, C. Makrides, and E. Tiesinga, “Challenges to miniaturizing cold atom technology for deployable vacuum metrology,” *Metrologia* **55**, S182 (2018).
- ¹⁰J. L. Booth, P. Shen, R. V. Krems, and K. W. Madison, “Universality of quantum diffractive collisions and the quantum pressure standard,” *New J. Phys.* **21**, 102001 (2019).
- ¹¹P. Shen, K. W. Madison, and J. L. Booth, “Realization of a universal quantum pressure standard,” *Metrologia* **57**, 025015 (2020).
- ¹²P. Shen, K. W. Madison, and J. L. Booth, “Refining the cold atom pressure standard,” *Metrologia* **58**, 022101 (2021).
- ¹³D. S. Barker, B. P. Acharya, J. A. Fedchak, N. N. Klimov, E. B. Norrgard, J. Scherschligt, E. Tiesinga, and S. P. Eckel, “Precise quantum measurement of vacuum with cold atoms,” *Rev. Sci. Instrum.* **93**, 121101 (2022).
- ¹⁴J. Klos and E. Tiesinga, “Elastic and glancing-angle rate coefficients for heating of ultracold Li and Rb atoms by collisions with room-temperature noble gases, H₂, and N₂,” *The Journal of Chemical Physics* **158**, 014308 (2023).
- ¹⁵D. S. Barker, J. A. Fedchak, J. Klos, J. Scherschligt, A. A. Sheikh, E. Tiesinga, and S. P. Eckel, “Accurate measurement of the loss rate of cold atoms due to background gas collisions for the quantum-based cold atom vacuum standard,” *AVS Quantum Science* **5**, 035001 (2023).
- ¹⁶C. Makrides, D. S. Barker, J. A. Fedchak, J. Scherschligt, S. Eckel, and E. Tiesinga, “Elastic rate coefficients for Li+H₂ collisions in the calibration of a cold-atom vacuum standard,” *Phys. Rev. A* **99**, 042704 (2019).
- ¹⁷C. Makrides, D. S. Barker, J. A. Fedchak, J. Scherschligt, S. Eckel, and E. Tiesinga, “Collisions of room-temperature helium with ultracold lithium and the van der Waals bound state of HeLi,” *Phys. Rev. A* **101**, 012702 (2020).
- ¹⁸C. Makrides, D. S. Barker, J. A. Fedchak, J. Scherschligt, S. Eckel, and E. Tiesinga, “Erratum: Collisions of room-temperature helium with ultracold lithium and the van der Waals bound state of HeLi,” *Phys. Rev. A* **105**, 029902 (2022).
- ¹⁹C. Makrides, D. S. Barker, J. A. Fedchak, J. Scherschligt, S. Eckel, and E. Tiesinga, “Erratum: Elastic rate coefficients for Li+H₂ collisions in the calibration of a cold-atom vacuum standard,” *Phys. Rev. A* **105**, 039903 (2022).
- ²⁰R. A. Stewart, P. Shen, J. L. Booth, and K. W. Madison, “Measurement of Rb-Rb van der Waals coefficient via quantum diffractive universality,” *Phys. Rev. A* **106**, 052812 (2022).
- ²¹L. H. Ehinger, B. P. Acharya, D. S. Barker, J. A. Fedchak, J. Scherschligt, E. Tiesinga, and S. Eckel, “Comparison of two multiplexed portable cold-atom vacuum standards,” *AVS Quantum Sci.* **4**, 034403 (2022).
- ²²P. Shen, E. Frieling, K. R. Herperger, D. Uhlend, R. A. Stewart, A. Deshmukh, R. V. Krems, J. L. Booth, and K. W. Madison, “Cross-calibration of atomic pressure sensors and deviation from quantum diffractive collision universality for light particles,” *New J. Phys.* **25**, 053018 (2023).

- ²³A. Deshmukh, R. A. Stewart, P. Shen, J. L. Booth, and K. W. Madison, “Trapped-particle evolution driven by residual gas collisions,” *Phys. Rev. A* **109**, 032818 (2024).
- ²⁴V. Bagnato, D. E. Pritchard, and D. Kleppner, “Bose-Einstein condensation in an external potential,” *Phys. Rev. A* **35**, 4354 (1987).
- ²⁵O. J. Luiten, M. W. Reynolds, and J. T. M. Walraven, “Kinetic theory of the evaporative cooling of a trapped gas,” *Phys. Rev. A* **53**, 381 (1996).
- ²⁶C. Pethick and H. Smith, [Bose-Einstein Condensation in Dilute Gases](#) (Cambridge University Press, 2002).
- ²⁷DLMF, “*NIST Digital Library of Mathematical Functions*,” <https://dlmf.nist.gov/>, Release 1.2.1 of 2024-06-15, f. W. J. Olver, A. B. Olde Daalhuis, D. W. Lozier, B. I. Schneider, R. F. Boisvert, C. W. Clark, B. R. Miller, B. V. Saunders, H. S. Cohl, and M. A. McClain, eds.
- ²⁸Note that in Ref. 15 for practical reasons, $\eta_S(t)$ was the ratio of the measured atom number in the magnetic trap after time t to the atom number in the magneto-optical trap (MOT) just before transfer into the magnetic trap.
- ²⁹D. Barker, E. Norrgard, N. Klimov, J. Fedchak, J. Scherschligt, and S. Eckel, “Single-beam Zeeman slower and magneto-optical trap using a nanofabricated grating,” *Phys. Rev. Applied* **11**, 064023 (2019).
- ³⁰N. Oceanic and A. Administration, “Surface gravity prediction,” https://www.ngs.noaa.gov/cgi-bin/grav_pdx.prl.

Supplemental tables for “On the effect of ‘glancing’ collisions in the cold atom vacuum standard”

Stephen P. Eckel ^{1, a)} Daniel S. Barker ¹ James A. Fedchak ¹ Jacek Kłos ^{2, 3} Julia Scherschligt ¹ and Eite Tiesinga ^{2, 3, 4}

¹⁾*Sensor Science Division, National Institute of Standards and Technology, Gaithersburg, Maryland 20899, USA*

²⁾*Joint Quantum Institute, College Park, Maryland 20742, USA*

³⁾*Physics Department, University of Maryland, College Park, Maryland, 20742, USA*

⁴⁾*Quantum Measurement Division, National Institute of Standards and Technology, Gaithersburg, Maryland 20899, USA*

(Dated: 18 September 2024)

Here, we present several additional tables of including sample uncertainty budgets, shifts in values of this work compared to past work, and updated ⁸⁷Rb loss rate coefficients across multiple different methods.

¹D. S. Barker, J. A. Fedchak, J. Kłos, J. Scherschligt, A. A. Sheikh, E. Tiesinga, and S. P. Eckel, “Accurate measurement of the loss rate of cold atoms due to background gas collisions for the quantum-based cold atom vacuum standard,” *AVS Quantum Science* **5**, 035001 (2023).

²P. Shen, K. W. Madison, and J. L. Booth, “Refining the cold atom pressure standard,” *Metrologia* **58**, 022101 (2021).

³P. Shen, E. Frieling, K. R. Herperger, D. Uhlund, R. A. Stewart, A. Deshmukh, R. V. Krems, J. L. Booth, and K. W. Madison, “Cross-calibration of atomic pressure sensors and deviation from quantum diffractive collision universality for light particles,” *New J. Phys.* **25**, 053018 (2023).

⁴J. Kłos and E. Tiesinga, “Elastic and glancing-angle rate coefficients for heating of ultracold Li and Rb atoms by collisions with room-temperature noble gases, H₂, and N₂,” *The Journal of Chemical Physics* **158**, 014308 (2023).

	Type	Source	Contribution (%)
Experi- mental	B	Temperature of the CAVS, T	0.51
	B	Flowmeter, \dot{N}	0.24
	B	Orifice area, A	0.13
	B	Imaging non-linearity and drifts, Γ	0.07
	B	Pressure ratio, r_p	0.05
	B	Orifice transmission prob., α_{MC}	0.02
	B	Subtotal	0.59
A	Subtotal	0.73	
		Total	0.94
Theory	B	Temperature of the CAVS, T	0.32
	B	Theory	0.26
	B	Trap Depth, W	0.02
	B	Temperature of sensor atoms, T_S	0.01
	B	Isotopic shift	< 0.01
			Total

TABLE S1. Experimental and theoretical statistical (type-A) and systematic (type-B) uncertainty budgets of loss rate coefficient L for the p-CAVS with ⁷Li sensor atoms and a natural abundance Ar background gas. The experimental and theoretical contributions add in quadrature to the relative uncertainty $u(L)/L$ of L . The experimental and theoretical temperature contributions are correlated. See Ref. 1 on how this non-zero correlation is treated.

^{a)}Electronic mail: stephen.eckel@nist.gov

System	L (Ref. 1) $10^{-9}\text{cm}^3/\text{s}$	L (This work) $10^{-9}\text{cm}^3/\text{s}$	% shift
${}^7\text{Li}-{}^4\text{He}$	1.661(41)	1.662(41)	+0.06
${}^7\text{Li}-\text{Ne}$	1.55(14)	1.55(14)	+0.23
${}^7\text{Li}-\text{N}_2$	2.642(22)	2.651(22)	+0.34
${}^7\text{Li}-\text{Ar}$	2.3359(98)	2.3443(96)	+0.36
${}^7\text{Li}-\text{Kr}$	2.1398(71)	2.1503(68)	+0.49
${}^7\text{Li}-\text{Xe}$	2.234(21)	2.249(21)	+0.64

TABLE S2. Shift in the theoretically predicted values of the loss rate coefficient L for various natural abundance gases colliding with ultracold ${}^7\text{Li}$ between Ref. 1 and this present work. Numbers in parentheses are one-standard-deviation, $k = 1$ uncertainties.

Type	Source	Contribution (%)
Experi- mental	B Flowmeter, \dot{N}	0.26
	B Orifice area, A	0.13
	B Imaging non-linearity and drifts, Γ	0.07
	B Temperature of the sensor atoms, T_S	0.06
	B Pressure ratio, r_p	0.05
	B Temperature of the CAVS, T	0.04
	B Orifice transmission prob., α_{MC}	0.02
	B Trap depth, W	< 0.01
	B Subtotal	0.31
A Subtotal	1.56	
Total		1.59
Theory	B Theory	0.23
	B Temperature of the CAVS, T	0.02
	B Isotopic shift	< 0.01
	Total	0.23

TABLE S3. Experimental and theoretical statistical (type-A) and systematic (type-B) uncertainty budgets of zero-trap depth loss rate coefficient K for the I-CAVS with ${}^{87}\text{Rb}$ sensor atoms and a natural abundance Ar background gas. The experimental and theoretical contributions add in quadrature to the relative uncertainty $u(K)/K$ of K . The experimental and theoretical temperature contributions are correlated. See Ref. 1 on how this non-zero correlation is treated.

System	K ($10^{-9}\text{cm}^3/\text{s}$)			a_{gl} ($10^{-7}\text{cm}^3/[\text{s K}]$)			b_{gl} ($10^{-5}\text{cm}^3/[\text{s K}^2]$)		
	Ref. 1	This work	% shift	Ref. 1	This work	% shift	Ref. 1	This work	% shift
${}^{87}\text{Rb}-{}^4\text{He}$	2.34(6)	2.35(6)	+0.4	0.1(8)	-0.4(8)	-130	—	—	—
${}^{87}\text{Rb}-\text{Ne}$	2.23(5)	2.21(5)	-0.7	1.3(7)	1.2(7)	-6.7	2.6(2.4)	2.0(3.5)	-30
${}^{87}\text{Rb}-\text{N}_2$	3.60(1)	3.56(8)	-1.0	2.3(1.4)	1.9(1.5)	-21	13.3(8.4)	5.8(7.2)	-130
${}^{87}\text{Rb}-\text{Ar}$	3.30(6)	3.29(5)	-0.6	2.3(8)	2.6(8)	+7.0	-1.0(2.9)	-2.4(3.9)	-58
${}^{87}\text{Rb}-\text{Kr}$	2.83(4)	2.80(4)	-0.8	1.9(5)	1.8(5)	-6.3	3.8(2.7)	3.8(2.5)	0
${}^{87}\text{Rb}-\text{Xe}$	2.93(7)	2.87(6)	-2.0	3.9(9)	3.5(1.0)	-11	10.3(3.0)	12.8(4.5)	+23

TABLE S4. Shift in the experimentally determined values of the loss rate coefficient K at zero trap depth, the first-order glancing rate coefficient a_{gl} , and the second-order glancing rate coefficient b_{gl} for various natural abundance gases colliding with ultracold ${}^{87}\text{Rb}$ between Ref. 1 and this present work. Numbers in parentheses are one-standard-deviation, $k = 1$ uncertainties.

System	K (10^{-9} cm ³ /s)			
	UQDC ²	Ratiometric ³	Theory ⁴	This work
⁸⁷ Rb-H ₂	5.12(15)	3.8(2)	3.9(1)	—
⁸⁷ Rb- ⁴ He	2.41(14)	—	2.37(3)	2.35(6)
⁸⁷ Rb-Ne	—	—	2.0(2)	2.21(5)
⁸⁷ Rb-N ₂	3.14(5)	—	3.45(6)	3.56(8)
⁸⁷ Rb-Ar	2.79(5)	—	3.035(7)	3.29(5)
⁸⁷ Rb-CO ₂	2.84(6)	—	—	—
⁸⁷ Rb-Kr	—	—	2.79(1)	2.80(4)
⁸⁷ Rb-Xe	2.75(4)	—	2.88(1)	2.87(6)

TABLE S5. Comparison of this work with published measurements, including those utilizing universality of quantum diffractive collisions (UQDC), and theoretical calculations of ⁸⁷Rb-X loss rate coefficients. Numbers in parentheses are one-standard-deviation, $k = 1$ uncertainties. For simplicity, the statistical and systematic uncertainties from Ref. 2 are added in quadrature. For the theory and this work, $T = 295.2(3)$ K. For Ref. 2, $T = 294$ K.